

Numerical Study of the Sand Movement around a Cylindrical Body Standing on the Sand*

Makiko KAN**, Tetuya KAWAMURA***
and Kunio KUWAHARA****

The flow around a cylindrical body standing on the sand is computed numerically and the movement of the sand is investigated. The numerical method employed in this study can be divided into three parts: (1) calculation of the flow around the pole using the marker and cell (MAC) method with a generalized coordinate system; (2) estimation of the sand transfer caused by the flow through friction; (3) determination of the shape of the ground. Since the computational area changes at step (3), this procedure has to be repeated at each time step. Results show that the horseshoe vortex scoops out the ground in front of the pole. When the pole stands vertically on a flow, it generates a big horseshoe vortex to make the scouring force strong. On the other hand, when the pole has a cross section that is flatter along the flow, such as a lens or ellipse, the scouring force becomes weaker. Furthermore, it is found that the horseshoe vortex becomes smaller when the pole has a conical base.

Key Words: Computational Fluid Dynamics, Numerical Analysis, Finite Difference Method, Sand Transfer by Wind, Cylindrical Body, Horseshoe Vortex

1. Introduction

It is often observed that the ground in front of a pier is scooped by the flow. This phenomenon is called scour due to flow. Since the scours around piers weaken the bridge, it is necessary to investigate its mechanism. The origin of this phenomenon is the formation of the vortex around the pier. In general, a U-shape vortex is generated in the upstream side of a pole standing on a flat plate (Fig. 1). This vortex is called a horseshoe vortex from its shape. This vortex scoops the ground in front of the pole.

The authors simulated the scour around a circular cylinder numerically in the previous work⁽¹⁾. The results revealed the existence of the horseshoe vortex and it was found that this vortex scoops the ground along the axis of the vortex. The agreement between the results of the computation and the experimental data was satisfactory and we concluded that the computation a good tool to understand the mechanism

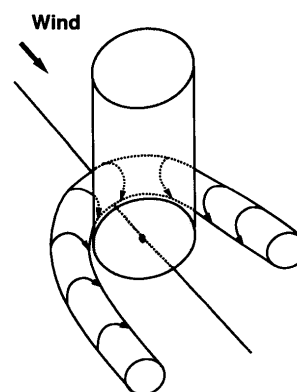


Fig. 1 Schematic figure of the horseshoe vortex generated by a circular cylinder

* Received 12th March, 2001. Japanese original: Trans. Jpn. Soc. Mech. Eng., Vol. 66, No. 646, B (2000), pp. 1266-1272 (Received 12th October, 1999)

** Showa High School, Azuma Akishima, Tokyo 196-0033, Japan

*** Graduate School of Humanities and Sciences, Ochanomizu University, Ootsuka, Bunkyo-ku, Tokyo 112-8610, Japan. E-mail: kawamura@ns.is.ocha.ac.jp

**** The Institute of Space and Astronautical Science, Sagamihara, Kanagawa 229-8510, Japan

of this type of flow.

The objective of the present study is to develop the previous work and to apply it to more practical problems. Namely, the sand movement around various cylindrical bodies such as a square cylinder and triangular cylinder is numerically simulated and the effects of the shape of the pole on the formation of the horseshoe vortex and the scour are investigated. These results are directly applicable to the design of the pier of a bridge.

2. Numerical Method

The numerical method is similar to that employed in the previous work⁽¹⁾. In this study, it is assumed that the cylindrical body is standing on the sand and the sand is transferred by the wind. This phenomenon is analogous to that of a pier standing in a river.

The method consists of two parts, i.e. the computation of the sand movement and that of the flow field around the body, and they are repeated alternatively. Concretely, the following three steps are repeated:

(1) Computation of the flow field around the cylindrical body standing on the sand.

(2) Calculation of the surface friction due to the flow and estimation of the sand transfer by the friction.

(3) Computation of the shape of the sand surface.

The time evolution of the sand surface can be obtained by iterative computation from (1) to (3). The flow field depends on the shape of the computational region which is changed by step (3). Both the flow field and the shape of the sand surface are determined at every time step while interacting with each other. Details of the computation are explained later on.

2.1 Computation of the flow field around the cylindrical body

Strictly speaking, the Reynolds number of the actual flow is high enough that the flow is in the turbulence regime and it is necessary to compute turbulent flow over the complex geometry. However, there are large separations of the flow behind the cylinder and it is difficult to find a suitable turbulence model by which the turbulent flow with large separation can be simulated adequately. In this study, we assume that the flow is laminar and the effect of the turbulence can be incorporated into the calculation through the eddy viscosity of constant value for the first step of the numerical study. In other words, we calculate the flow at a rather low Reynolds number instead of computing the mean turbulent flow. Actually, in the previous study, we computed the laminar flows around the circular cylinder at $Re=10^3$ and we found the formation of a horseshoe vortex which also

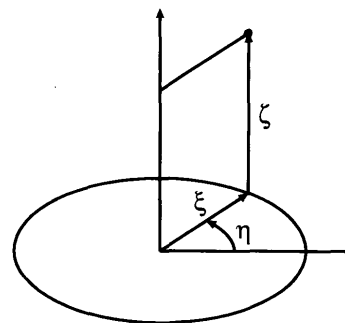


Fig. 2 Definition of variables

plays a dominant role in this study. In addition, the shape of the sand surface around the circular cylinder obtained in the previous work agrees well with the experimental result.

Taking these considerations into account, we also compute the laminar flow of $Re=10^3$ in this study. The basic equations are the incompressible Navier-Stokes equations:

$$\text{div } \mathbf{u} = 0 \quad (1)$$

$$\frac{\partial \mathbf{u}}{\partial t} + (\mathbf{u} \cdot \nabla) \mathbf{u} = -\frac{1}{\rho} \nabla p + \nu \nabla^2 \mathbf{u} \quad (2)$$

Equation (1) is the continuity equation and Eq. (2) is the momentum equation. The standard MAC method is employed to solve the above three-dimensional equations. The time-dependent generalized coordinate system (Fig. 2) is used in order to express the complicated sand surface which will change in time precisely. This enabled us to perform the computation on a fixed rectangular grid.

The transformed equation is approximated by a finite difference method. All the spatial derivatives except for the nonlinear terms of Eq. (2) are approximated by the second order central difference. A third order upwind difference is employed for the discretization of the nonlinear terms. The Euler explicit method is used for the time integration.

Initially, the flow field is assumed to be uniform in all the regions, i.e. $u=10$ m/s, $v=0$ and $w=0$ are used as the initial conditions of the computation. The boundary conditions are as follows:

On the sand surface: no-slip condition
($u=v=w=0$)

On the cylindrical body: no-slip condition
($u=v=w=0$)

On the upper boundary: free-slip condition
($\frac{\partial u}{\partial z} = \frac{\partial v}{\partial z} = 0, w=0$)

Infinity: uniform flow ($u=10.0, v=w=0$)

2.2 Estimation of the sand transfer

There are three types of sand transfer by wind, i.e. suspension, saltation and surface creep⁽³⁾⁻⁽⁵⁾. In suspension, small grains approximately in 0.1 - 0.05

mm diameter are wafted or drifted in the air and fly over a considerably long distance. This is one of the major processes of the movement of other sands in China. In saltation, a flying grain strikes another grain on the ground and makes it jump up. This process continuously takes place and finally the sands are transferred downstream. The size of the grain in this process is between 0.2 and 0.3 mm and the grain flies about 10 cm - 100 cm in one jumping motion. On the other hand, a large grain rolls over or creeps along the surface, known as the process of surface creep. In the area where sand dunes of various shapes exist, the sands move vigorously and most of the grains are size of 0.2 - 0.3 mm⁽³⁾. Therefore, it is considered that the major process responsible for the formation of a typical sand dune is saltation. Bagnold proposed the following relationship between the surface friction velocity u_* and sand transfer q ⁽³⁾.

$$q = c_1 \frac{\rho}{g} u_*^3 \quad (3)$$

Kawamura⁽⁴⁾ and Lettau⁽⁵⁾ also proposed the following formulae respectively.

$$q = \begin{cases} c_2 \frac{\rho}{g} (u_* - u_{*t})(u_* + u_{*t})^2, & u_* > u_{*t}, \\ 0, & u_* \leq u_{*t} \end{cases} \quad (4)$$

$$q = \begin{cases} c_3 \frac{\rho}{g} u_*^2 (u_* - u_{*t}), & u_* > u_{*t}, \\ 0, & u_* \leq u_{*t} \end{cases} \quad (5)$$

The constants c_1, c_2, c_3 are determined by the experiments and u_{*t} (~ 0.2 m/s) in Eqs. (4) and (5) is critical friction velocity over which the sands begin to move. The velocity u_{*t} is defined by

$$u_{*t} = \sqrt{v \frac{du}{dz}} \quad (6)$$

It is shown from the various experiments⁽³⁾⁻⁽⁵⁾ that the velocity profile obeys the logarithmic law:

$$u = \frac{u_*}{\kappa} \log\left(\frac{z}{d}\right) \quad (7)$$

where κ is the Karman constant (~ 0.4) and d is the roughness factor of the sand surface which is considered to be about 1/30 of the diameter of the grain of the sand. Equation (7) can be used to calculate u_{*t} by giving the velocity u at some location z . However, since the turbulence model is not employed in this study, the use of Eq. (7) is questionable. Therefore, we utilize Eq. (6) to determine u_{*t} . It is shown from the experiments and simple theory^{(4),(5)} that the sand transfer by surface creep is estimated as about 1/4 of q although the constants in Eqs. (3) - (5) may be slightly changed in this case.

While Eq. (3) is used in the previous work⁽¹⁾, Eq. (5) is employed in this study. However, a large difference between both results of the calculations is not observed. The reason for this small difference is

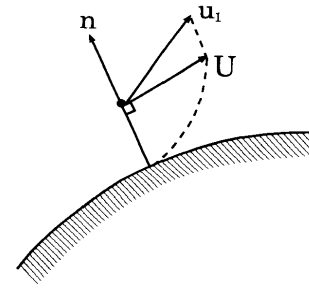


Fig. 3 Definitions of U , u_t and n

that u_* is large compared with u_{*t} and Eq. (5) is well approximated by Eq. (3).

Since the sand surface is two-dimensional, the quantity q is expressed in the vector form. Therefore Eq. (5) is extended to two-dimensional form as:

$$\mathbf{q} = c \frac{\rho}{g} |\mathbf{u}_*| \mathbf{u}_* (|\mathbf{u}_*| - u_{*t}) \quad (8)$$

Following the Ref. (6), the constant c in Eq. (8) is set to 5.5. Similarly, the friction velocity obtains the two-dimensional form as

$$|\mathbf{u}_*| = \sqrt{\nu (\nabla |\mathbf{U}| \cdot \mathbf{n}), \mathbf{u}_* // \mathbf{U}} \quad (9)$$

where \mathbf{n} is the unit normal to the surface and is calculated from

$$\nabla \zeta / |\nabla \zeta|$$

The velocity \mathbf{U} in Eq. (9) is parallel to the sand surface and is computed from

$$\mathbf{U} = \mathbf{u}_1 - (\mathbf{u}_1 \cdot \mathbf{n}) \mathbf{n} \quad (10)$$

where \mathbf{u}_1 is the velocity of the nearest grid point to the surface (Fig. 3). The quantity $\nabla |\mathbf{U}| \cdot \mathbf{n}$ equals $\partial |\mathbf{U}| / \partial n$.

2.3 Calculation of the surface shape

The sand is transferred according to Eq. (8) and the shape of the sand is changed. The shape of the sand surface is calculated by considering the conservation of the sand along the surface. If we employ a local coordinate system which lies on the surface and define the x -direction as X (direction of main flow), and y -direction as Y (spanwise direction), then the following relationship is obtained from the mass conservation law.

$$\rho_s \frac{dh}{dt} = -\frac{\partial q_1}{\partial X} - \frac{\partial q_2}{\partial Y} \quad (11)$$

Here, h is the normal distance from the sand surface, ρ_s is the sand density, and (q_1, q_2) are the X and Y components of \mathbf{q} . This relationship is derived by considering small control volume along the surface and equating the increment of h per unit time to the net mass influx into the volume. By using Eq. (11), the increment Δh during Δt is computed. Therefore, by adding this Δh to the height of the surface at n time step, the new height at $n+1$ time step is obtained. Namely, the grid point that expresses the sand surface is shifted along the ζ -axis upward or downward corresponding to the ζ component of Δh . After this

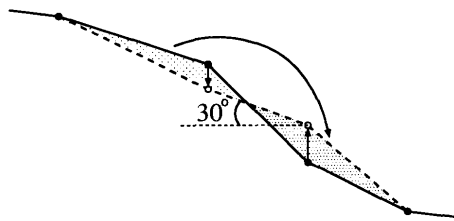


Fig. 4 Schematic figure of avalanche
(—before avalanche, --after avalanche)

movement, the mesh of the whole region is reconstructed.

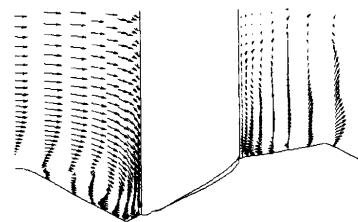
The slope of the sand surface has a maximum angle. If the slope exceeds this value, the sand slips down so as to keep this angle. The value of this angle is about 30 degrees although it depends slightly on the size of the grain or the condition of the surface such as wet or dry. In order to simulate this situation, the slope of the sand is monitored at each grid point during the calculation. If it exceeds the maximum angle, the height of the sand surface at the grid point is changed artificially both to keep the maximum value and to satisfy the observation of the sand (Fig. 4).

3. Results and Discussions

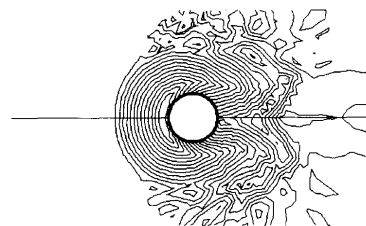
3.1 The effect of the shape of the cross section

The number of grid points in all computations is $64 \times 64 \times 64$. Uniform grids are used in the circumferential direction while nonuniform grids that are concentrated near the pole and the sand surface are employed in the radial and axial directions. The minimum grid size is 0.1 m and 0.018 m in the radial and axial directions, respectively. The number of grid points is determined after the test calculation using $96 \times 96 \times 96$. We confirmed that no major difference of results exists between fine and coarse grids. The shape of the far boundary is a circular cylinder whose diameter is 15 m and the upper boundary is at a height of 15 m. The eddy viscosity ν is set to $0.01 \text{ m}^2/\text{s}$. We also computed the sand movement by changing eddy viscosity from 0.0001 to $0.1 \text{ m}^2/\text{s}$ and found that there is no essential difference in the shape of the sand surface. The time increment is 0.001 sec and all the following results are obtained after 2 000 sec.

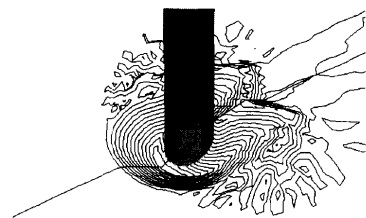
Figure 5 is the result for the circular cylinder whose diameter is 1 m. Figure 5(a) shows the velocity vectors in the cross section of $y=0$ (which corresponds to the solid line in Fig. 5(b)). The region of circulation appears on the upstream side near the cylinder and the sand surface. This shows the cross section of a horseshoe vortex which scoops the ground. Figures 5(b) and (c) are the top view and bird's eye view of the surface contours respectively.



(a) Velocity vectors in $y=0$ plane



(b) Surface contours (top view)



(c) Surface contours (bird's eye view)

Fig. 5 Circular cylinder $z_{\min} = -0.55 \text{ m}$, $z_{\max} = 0.26 \text{ m}$

From these figures, it is clear that the ground is scooped along the axis of the horseshoe vortex. In the caption of Figs. 8 - 11, the maximum value z_{\max} and minimum value z_{\min} of the surface are given. In this case, the minimum value (i.e. the depth of the deepest point) is -0.55 m .

It is anticipated that the wider the area of the plane perpendicular to the flow direction is, the stronger the horseshoe vortex formed. Figures 6 and 7 are the results of the triangular cylinder whose side length is 1 m. In Fig. 6, the wind strikes the corner of the triangle while it strikes the side of the triangle in Fig. 7. In the former situation, the horseshoe vortex is weak since the flow can pass away easily along both sides of the triangle. With time, the ground is scooped to form the scour which is analogous to that around the circular cylinder. However, the value of z_{\min} is -0.43 . This is shallower than that of a circular cylinder. On the other hand, in the case of Fig. 7, the flow strikes perpendicularly to the side plane to make a rather strong horseshoe vortex. As a result, the ground is scooped deeper than the case of Fig. 6. Taking this into account, it is clear that the ground is easily scooped around a cylindrical body which has a

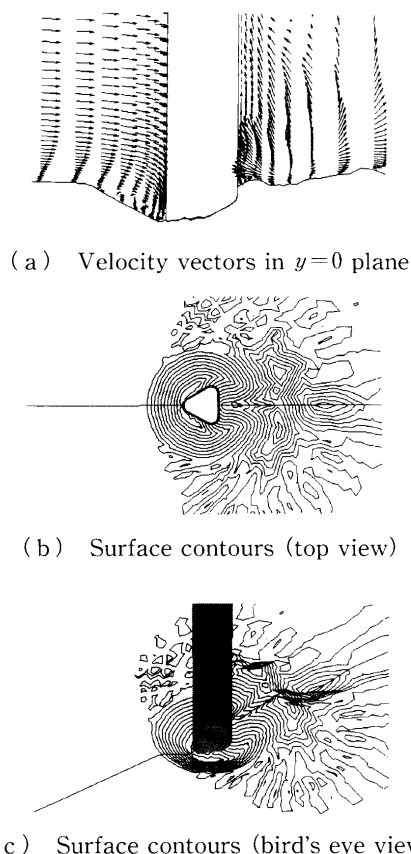


Fig. 6 Triangular cylinder $z_{\min} = -0.43$ m, $z_{\max} = 0.30$ m

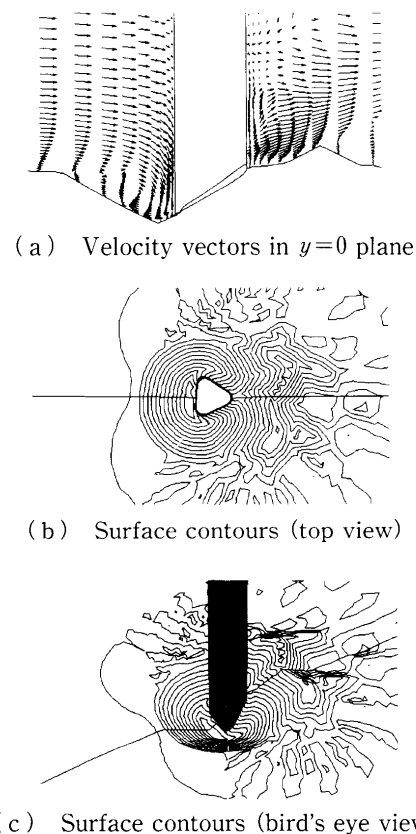


Fig. 7 Triangular cylinder (flow direction is 120°)
 $z_{\min} = -0.60$ m, $z_{\max} = 0.31$ m

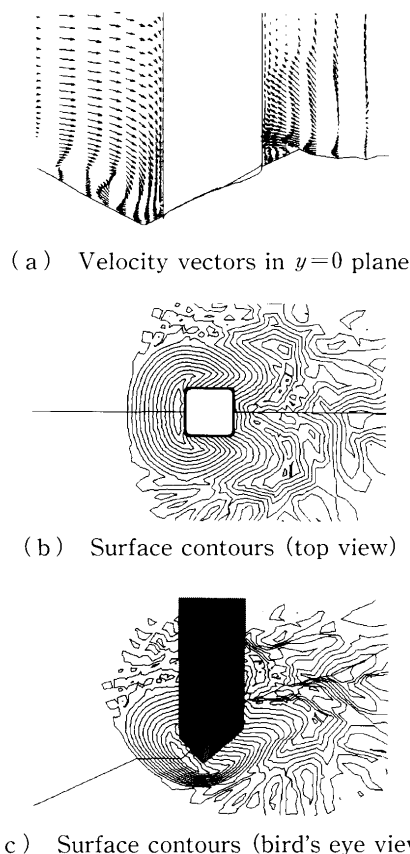


Fig. 8 Square cylinder $z_{\min} = -0.59$ m, $z_{\max} = 0.36$ m

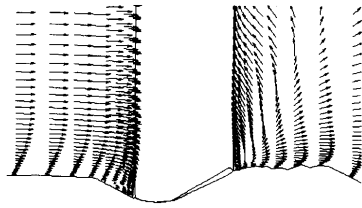
wide front surface. Figure 8 is the result for the square cylinder. We can see the same tendency.

It is effective to use a streamlined body in order to make the scour small. For example, Fig. 9 shows the results for a lenticular cylinder. The depth of the scour reduced to up to $3/5$ of that around a circular cylinder.

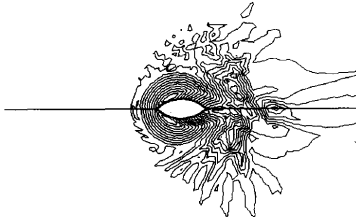
3.2 The effect of a conical base fixed on the cylinder

In the previous paper⁽¹⁾, the sand movement around a yawed cylinder is computed and the effect of the yaw angle on the sand transfer is studied. As a result, the scour of the upstream side becomes smaller when the circular cylinder is inclined leeward. From this result, the cylindrical body with the conical base is considered to make the scour smaller.

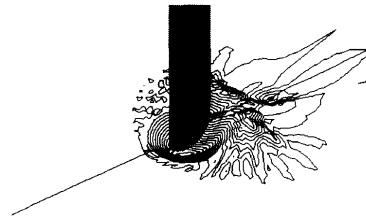
Figure 10 is the result for an elliptical cylinder whose long and short axes are 1 m and 0.5 m respectively. Since the cross section is elliptical (i.e. smooth curve), the horseshoe vortex is weak. Actually, the depth of the scour is -0.39 m which is smaller than that around a square cylinder. On the other hand, Fig. 11 is the result for the elliptical cylinder with a conical base. The base of this cylinder spreads from the height of 1 m with the slope of 60 degree as is shown in the figure. In this case, the depth of the scour



(a) Velocity vectors in $y=0$ plane

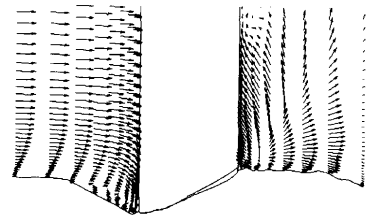


(b) Surface contours (top view)

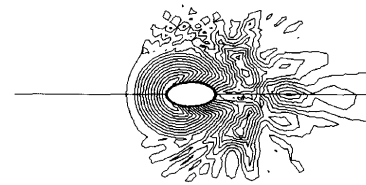


(c) Surface contours (bird's eye view)

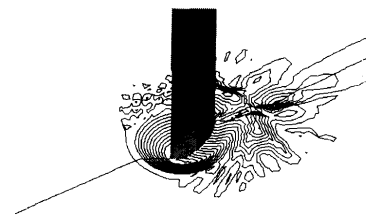
Fig. 9 Lenticular cylinder $z_{\min} = -0.30$ m, $z_{\max} = 0.22$ m



(a) Velocity vectors in $y=0$ plane

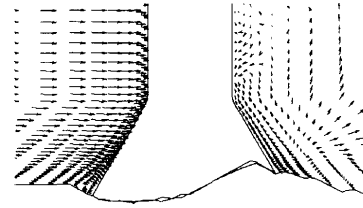


(b) Surface contours (top view)

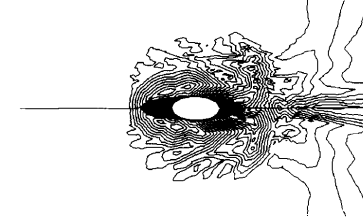


(c) Surface contours (bird's eye view)

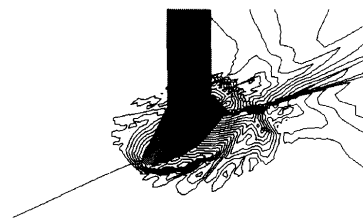
Fig. 10 Elliptic cylinder $z_{\min} = -0.39$ m, $z_{\max} = 0.24$ m



(a) Velocity vectors in $y=0$ plane



(b) Surface contours (top view)



(c) Surface contours (bird's eye view)

Fig. 11 Elliptic cylinder with conical base $z_{\min} = -0.27$ m, $z_{\max} = 0.30$ m

reduces up to -0.24 m. It is considered that the flow is curved upward which suppress the formation of the horseshoe vortex. In addition to the advantage mentioned here, the stability of the pier also increases by the use of a conical base. Therefore, it is concluded that a cylindrical body with a conical base as is shown in Fig. 11 is appropriate for the pier of the bridge.

4. Conclusions

In this study, the previous study on sand movement around the circular cylinder has been extended and flows around various cylindrical bodies have been applied. The results are compared with each other and the following conclusions are obtained:

(1) The ground is scooped by the flow strongly when the cylindrical body has a flat plane perpendicular to the flow. This is because that the horseshoe vortex is easily formed for this kind of cylinder. On the other hand, the scour is smaller when the cylindrical body has a curved plane such as lenticular or elliptical shape.

(2) For the cylindrical body with conical base, the flow is curved upward and the formation of the horseshoe vortex is suppressed. Therefore, this kind of shape prevents scour formation and is more

suitable for the pier of a bridge.

The size-grading of the grains by wind may play an important role, for example, in the process when the sands form various types of dunes. However, in this study, we can clarify the feature of the sand movement around the cylindrical body by simply relating the sand transfer to the surface friction and moving the sand uniformly. Although the effect of the turbulence is only incorporated into the computation through the simplest eddy viscosity model, we can obtain the qualitative difference among various shapes of the cylindrical body. From these results, we can conclude that the present method can be applied to an actual problem from the qualitative point of view.

References

- (1) Kawamura, T., Kan, M. and Hayashi, T., Numerical Study of the Flow and the Sand Movement around a Circular Cylinder Standing on the Sand, *JSME Int. J., Ser. B*, Vol. 42, No. 4 (1999), pp. 605-611.
- (2) Kawamura, T. and Kuwahara, K., Computation of High Reynolds Number Flow around a Circular Cylinder with Surface Roughness, *AIAA Paper*, 84-0340 (1984).
- (3) Bagnold, R.A., The Movement of Desert Sand, *Proc. Roy. Soc.*, A157 (1936), pp. 594-620.
- (4) Kawamura, R., Study on Sand Movement by Wind, *Rept. Inst. Sci. Technol., Univ. Tokyo*, (in Japanese), Vol. 5 (1951), pp. 95-112.
- (5) Nagashima, H., Sand Transport and Dunes in Deserts, *J. Japan Society of Fluid Mechanics*, (in Japanese), Vol. 10, No. 33 (1991), pp. 166-180.
- (6) Wipperman, F.K. and Gross, G., The Wind-induced Shaping and Migration of an Isolated Dune—A Numerical Experiment—, *Boundary-Layer Meteorol.*, Vol. 36 (1986), pp. 319-334.